



This is a repository copy of *Structural and thermophysical behaviour of barium zinc aluminoborosilicate glasses for potential application in SOFCs*.

White Rose Research Online URL for this paper:  
<https://eprints.whiterose.ac.uk/180892/>

Version: Accepted Version

---

**Article:**

Grema, L.U. and Hand, R.J. [orcid.org/0000-0002-5556-5821](https://orcid.org/0000-0002-5556-5821) (2021) Structural and thermophysical behaviour of barium zinc aluminoborosilicate glasses for potential application in SOFCs. *Journal of Non-Crystalline Solids*, 572. 121082. ISSN 0022-3093

<https://doi.org/10.1016/j.jnoncrysol.2021.121082>

---

Article available under the terms of the CC-BY-NC-ND licence  
(<https://creativecommons.org/licenses/by-nc-nd/4.0/>).

**Reuse**

This article is distributed under the terms of the Creative Commons Attribution-NonCommercial-NoDerivs (CC BY-NC-ND) licence. This licence only allows you to download this work and share it with others as long as you credit the authors, but you can't change the article in any way or use it commercially. More information and the full terms of the licence here: <https://creativecommons.org/licenses/>

**Takedown**

If you consider content in White Rose Research Online to be in breach of UK law, please notify us by emailing [eprints@whiterose.ac.uk](mailto:eprints@whiterose.ac.uk) including the URL of the record and the reason for the withdrawal request.



[eprints@whiterose.ac.uk](mailto:eprints@whiterose.ac.uk)  
<https://eprints.whiterose.ac.uk/>

# Structural and Thermophysical Behaviour of Barium Zinc Aluminoborosilicate Glasses for Potential Application in SOFCs

Lawan U. Grema<sup>1</sup> and Russell J. Hand<sup>2</sup>

*Department of Materials Science and Engineering, University of Sheffield, Sir Robert Hadfield Building, Mappin Street, Sheffield, S1 3JD, UK*

## Abstract

Structure property relationships in two series of BaO-ZnO-La<sub>2</sub>O<sub>3</sub>-Al<sub>2</sub>O<sub>3</sub>-B<sub>2</sub>O<sub>3</sub>-SiO<sub>2</sub> glasses have been investigated to assess their suitability for use as sealants in solid oxide fuel cell (SOFC) applications. Density, mechanical properties, thermal and electrical properties have been investigated as a function of composition. Raman and Fourier transfer infra-red spectroscopies were undertaken to obtain insights into the glass structure. The mechanical properties are generally relatively high but the thermal expansion coefficients are lower than ideal for SOFC sealants. Of the glasses studied 9.74BaO-6.39ZnO-15.84La<sub>2</sub>O<sub>3</sub>-5.04Al<sub>2</sub>O<sub>3</sub>-15.63B<sub>2</sub>O<sub>3</sub>-47.37SiO<sub>2</sub> (mol%) has the most promising properties for SOFC sealing applications.

## 1. Introduction

Solid oxide fuel cells (SOFCs) are devices with great potential for the conversion of chemical energy into electrical energy [1,2]. They typically operate at elevated temperatures of between 600 and 1000°C [3,4,5] in oxidizing, reducing and humid environments [6], with required service lives of 5000 h in mobile applications [7] and 50000 to 75000 hours for stationary applications [7,8]. SOFCs may have a planar or a tubular structure [1,2,3,4,5,9] with planar SOFCs (pSOFCs) being preferred as they can generate higher current outputs, because the current paths are shorter [6,9]; they are also easier to manufacture. However pSOFCs require hermetic sealing to function [4,5] and this hermetic sealing of the electrodes, electrolytes and metallic interconnects to prevent the fuel and oxidants mixing [10,11] remains a key challenge [12]. As well as being gas tight the hermetic sealing materials must have be electrically insulating; mechanically and chemically stable at high temperatures; and have chemical and thermal expansion compatibility with the other components of the SOFC [10,13]. Glass based sealants (whether glasses or glass-ceramics) are of interest because in general they are cheaper and have a greater resistance to dual atmospheres than metallic sealants. Glass based sealants can also be tailored compositionally to meet most of the sealing requirements with and have the advantage of better wetting to sealing interfaces [1,2,14].

Sealant glasses must have a glass transition temperature ( $T_g$ ) that lies below the SOFC operating temperature [1,2,4] and a thermal expansion coefficient (TEC) that closely matches the TECs of other cell components to avoid thermal expansion mismatch stresses [4]. Hence a range of aluminosilicate, borosilicate, borate and phosphate based glasses have been studied for these applications (see, for example, refs. [15,16]). However it has been found that compositions based on alkali silicates are not suitable because the alkalis have been found to react with the SOFC components [17]; borate and phosphate based glasses are also not suitable [16,18]. However aluminoborosilicate compositions that combine the effects of two glass forming oxides as well as a conditional glass former are attractive for this application, with Al<sub>2</sub>O<sub>3</sub> being useful for controlling crystallization and B<sub>2</sub>O<sub>3</sub> improving the wetting behaviour [19]. In addition La<sub>2</sub>O<sub>3</sub> has been shown to be useful as a viscosity modifier and TEC stabilizer [15], while BaO and ZnO both reduce  $T_g$  and the softening temperature,  $T_s$ , while raising TEC [9,15,19]. Hence we focus on the effects of varying the ZnO content of two

---

<sup>1</sup> Current address: Department of Mechanical Engineering, Ramat Polytechnic, Maiduguri, Nigeria

<sup>2</sup> E-mail: r.hand@sheffield.ac.uk

related series of barium zinc lanthanum aluminoborosilicate glasses on the thermal and mechanical properties of these glasses and related glass-ceramics.

## 2. Experimental

### 2.1 Glass melting and ceramisation

Two series of BaO-ZnO-La<sub>2</sub>O-Al<sub>2</sub>O<sub>3</sub>-B<sub>2</sub>O<sub>3</sub>-SiO<sub>2</sub> glasses were produced via the melt quench technique. In one series ZnO decreased while B<sub>2</sub>O<sub>3</sub> increased (ZnO-B<sub>2</sub>O<sub>3</sub> series) and in the other ZnO decreased while SiO<sub>2</sub> increased. While the specific glasses studied have not been previously reported the starting amounts of lanthanum oxide (15 mol%), alumina (5 mol%), boron oxide (10 mol%) and silica (45 mol%) reflect various compositions studied for SOFC applications (see, for example, [20,21]). The nominal compositions were originally designed to be 10BaO·(15 - x)ZnO·15La<sub>2</sub>O<sub>3</sub>·5Al<sub>2</sub>O<sub>3</sub>·(10 + x)B<sub>2</sub>O<sub>3</sub>·45SiO<sub>2</sub> (x = 0, 2.5, 5, 7.5 and 10 mol%; ZnO-B<sub>2</sub>O<sub>3</sub> series) and 10BaO·(20 - y)ZnO·15La<sub>2</sub>O<sub>3</sub>·5Al<sub>2</sub>O<sub>3</sub>·10B<sub>2</sub>O<sub>3</sub>·(45 + y)SiO<sub>2</sub> (y = 0, 2.5, 5 and 7.5 mol%; ZnO-SiO<sub>2</sub> series), however due to a spreadsheet error one of the atomic masses used in the original batch calculations was wrong and all of the batched compositions differed slightly from this initial design (see Table 1). In view of this glass codes are based on the *analysed* molar contents of ZnO, B<sub>2</sub>O<sub>3</sub> and SiO<sub>2</sub> with all other components being nominally constant. Hence the codes are of the form Z<sub>p</sub>B<sub>q</sub>S<sub>r</sub>, where p, q and r reflect the analysed molar contents of ZnO, B<sub>2</sub>O<sub>3</sub> and SiO<sub>2</sub> respectively (see Table 1).

Batches to produce 300 g of glass were prepared using SiO<sub>2</sub> (99.8%; Glassworks Services), H<sub>3</sub>BO<sub>3</sub> (99.5%; Sigma-Aldrich, UK), Al(OH)<sub>3</sub> (99.5%; Fisher Chemical, UK), BaCO<sub>3</sub> (99%; Fisher Chemical, UK) and ZnO (99.8%; Fisher Chemical, UK). The well mixed batch was transferred to a zirconia stabilized platinum crucible and heated to 1350°C in an electric furnace for a total of 5 h. After allowing 1 h to achieve a batch free melt a Pt stirrer was inserted into the melt and the melt was stirred during the remaining 4 h of melting. The molten glass was cast into a pre-heated steel mould. After demoulding the still hot glass was transferred to an annealing furnace where it was held at 650°C for 1 h and then cooled to room temperature at a rate of 1 °C min<sup>-1</sup>. Samples of the glasses were ceramised by subjecting them to a 50 h heat treatment at 800°C, which is representative of the operation temperature of intermediate SOFCs [22]. A relatively long heat treatment time of 50 h was chosen because of the very extended time SOFC sealant materials will spend at temperature.

Table 1: Analysed (XRF) and batched compositions in mol%.

Glass code	Analysed (batched) composition /mol%					
	BaO	ZnO	La <sub>2</sub> O <sub>3</sub>	Al <sub>2</sub> O <sub>3</sub>	B <sub>2</sub> O <sub>3</sub>	SiO <sub>2</sub>
<b>ZnO-B<sub>2</sub>O<sub>3</sub></b>						
Z <sub>18</sub> B <sub>9</sub> S <sub>45</sub>	9.60 (9.6)	17.63 (18.0)	14.17 (14.5)	5.11 (4.8)	8.87 (9.6)	44.61 (43.4)
Z <sub>15</sub> B <sub>10</sub> S <sub>46</sub>	9.03 (9.7)	15.12 (15.1)	15.52 (14.6)	5.10 (4.9)	9.55 (12.1)	45.69 (43.7)
Z <sub>10</sub> B <sub>13</sub> S <sub>48</sub>	8.79 (9.8)	9.82 (12.2)	14.98 (14.6)	5.62 (4.9)	12.61 (14.6)	48.18 (43.9)
Z <sub>9</sub> B <sub>14</sub> S <sub>48</sub>	10.05 (9.8)	8.56 (9.2)	14.33 (14.7)	4.78 (4.9)	14.30 (17.2)	47.99 (44.2)
Z <sub>6</sub> B <sub>16</sub> S <sub>47</sub>	9.74 (9.9)	6.39 (6.2)	15.84 (14.8)	5.04 (4.9)	15.63 (19.8)	47.37 (44.5)
<b>ZnO-SiO<sub>2</sub></b>						
Z <sub>23</sub> B <sub>9</sub> S <sub>40</sub>	10.37 (9.5)	23.04 (23.8)	13.54 (14.3)	4.80 (4.8)	8.60 (9.5)	39.65 (38.1)
Z <sub>21</sub> B <sub>8</sub> S <sub>43</sub>	9.75 (9.6)	20.59 (20.9)	13.70 (14.4)	4.81 (4.8)	8.10 (9.6)	43.05 (40.8)
Z <sub>18</sub> B <sub>9</sub> S <sub>45</sub>	9.37 (9.6)	18.34 (18.0)	14.16 (14.5)	4.42 (4.8)	8.64 (9.6)	45.07 (43.4)
Z <sub>14</sub> B <sub>9</sub> S <sub>48</sub>	9.32 (9.7)	14.11 (15.1)	14.33 (14.6)	4.78 (4.9)	9.45 (9.7)	48.01 (46.1)

## 2.2 Chemical and structural characterization

The chemical compositions of the glasses were measured by X-ray fluorescence (XRF) on a PanAnalytical Zetium instrument. Bulk cuboidal samples  $\sim 10 \times 10 \times 6$  mm were used. The  $B_2O_3$  content was obtained by difference. Uncertainties in the XRF data are conservatively estimated as major components except  $B_2O_3$  ( $\geq 10$  mol%)  $\pm 1$  mol%, intermediate components ( $\geq 1$  mol%)  $\pm 0.5$  mol% and minor components ( $< 1$  mol%)  $\pm 0.1$  mol%. As  $B_2O_3$  has been obtained by difference this gives an uncertainty of  $\pm 2$  mol% in the  $B_2O_3$  values. Sample densities were measured using an AccuPyc II 1340 pycnometer gas displacement system.

Powder X-ray diffraction (XRD) was used to verify whether the as prepared glasses were amorphous or not and also to verify the phases produced after heat treatment. Samples were crushed to a powder  $< 150$   $\mu\text{m}$  in size. Measurements were made using a Siemens D5000 diffractometer operated at 40 kV and 40 mA with  $\text{CuK}\alpha$  ( $\lambda=1.54056\text{\AA}$ ) radiation. The samples were scanned from  $15$ - $70$   $^\circ 2\theta$  with a step size of  $0.04$   $^\circ 2\theta$  and a scan rate of  $4.8$  s per step.

Differential thermal analysis (DTA) was used to determine  $T_g$  and any crystallization temperatures. DTA was undertaken using a Perkin Elmer STA8000. Approximately 40 mg of powdered glass and an equivalent weight of alumina as the inert reference were measured from room temperature to  $1000^\circ\text{C}$  at a heating rate of  $10$   $^\circ\text{C min}^{-1}$ . Given the tendency to crystallization only a single heating cycle was used with  $T_g$  being measured from the extrapolated onset of first endothermic peak in the DTA curve.

TEC values of the glasses and the ceramised samples were measured using a thermomechanical analyser (TMA). The samples were sliced into approximately  $10 \times 6 \times 6$  mm cuboids which were heated from RT to  $650^\circ\text{C}$  at  $1^\circ\text{C min}^{-1}$ .

Structural analysis was undertaken using Fourier transform infrared (FTIR) and Raman spectroscopies. For FTIR KBr pellets were prepared by mixing approximately 2 mg of glass with 200 mg of KBr in an agate mortar and then pressing into 13 mm diameter pellets using a Specac hydraulic press. The spectra of these pellets over the range  $400$  to  $4000$   $\text{cm}^{-1}$  were immediately measured using a Perkin-Elmer Frontier instrument, with a background scan being taken prior to measurement. Both transmittance and absorbance data were collected and peaks were assigned based on literature data.

Raman spectra were obtained using a Renishaw InVia Raman spectrometer using a  $514.5$  nm laser at a laser power of 20 mW. The laser beam was focused just beneath the polished surface via a  $50\times$  lens. The exposure and acquisition times were both 10 s. A baseline was fitted in the Wire 3.4 package by using the multiple spline curve option to connect points where the spectra goes to zero following the method of Colombari *et al.* [23]. The data was then corrected for temperature and frequency dependent scattering intensities using the Long correction method [24].

For mechanical testing glass samples were cut into  $20 \times 20 \times 10$  mm sections using a Secotom cutting machine with water-cooled diamond blade. The square faces of the samples were then successively ground and polished using SiC 400/ 600/ 800/ 1200 grit papers and 6/ 3/ 1  $\mu\text{m}$  diamond pastes. After polishing the samples were re-annealed at  $T_g$  for 1 h.

The elastic moduli of the glasses were measured using an ultrasonic pulse echo technique. Both the longitudinal ( $V_L$ ) and the transverse ( $V_T$ ) ultrasonic wave velocities were measured using an Olympus Epoch 6000. A 20 MHz longitudinal and a 5 MHz transverse transducer were used. An appropriate couplant was used to facilitate good contact between the transducer and the sample surface. To

minimize cumulative errors Young's modulus ( $E$ ), shear modulus ( $G$ ), bulk modulus ( $B$ ) and Poisson's ratio ( $\nu$ ) were all determined directly from the measured wave velocities using

$$E = \rho V_T^2 \frac{(3V_L^2 - 4V_T^2)}{(V_L^2 - V_T^2)} ; \quad (1)$$

$$G = \rho V_T^2 ; \quad (2)$$

$$B = \rho \frac{3V_L^2 - 4V_T^2}{3} ; \quad (3)$$

$$\nu = \frac{V_L^2 - 2V_T^2}{2(V_L^2 - V_T^2)} \quad (4)$$

respectively, where  $\rho$  is the measured density.

Hardness and indentation fracture toughness were measured using a Durascan micro/macro Vickers hardness tester. Hardness,  $H_V$ , was measured by applying a load of 9.81 N for 15 s and is given by

$$H_V = 1.8544 \frac{P}{d^2} , \quad (5)$$

where  $P$  is the load and  $d$  is the average diagonal length of the indents. Results are the mean of 13 to 15 hardness indentations in each case. For indentation fracture toughness indentations were made at loads of 2.943, 4.905, 9.81, 24.53 and 49.05 N. In each case the lengths of the median-radial cracks ( $2c$ ) originating from the corners of the indent were measured immediately after the indentation was made. Indentation fracture toughness was then calculated using

$$K_{Ic}^{indent} = \frac{0.0824P}{c^{3/2}} , \quad (6)$$

as Ponton and Rawlings have demonstrated that this equation gives results that correlate with more conventional fracture toughness measurements [25]. The ratio of hardness and indentation fracture toughness was used as a measure of brittleness,  $B_r$ :

$$B_r = \frac{H_V}{K_{Ic}^{indent}} . \quad (7)$$

AC impedance spectroscopy was used to measure the electrical properties of the glass and glass-ceramic samples. The impedance was measured using an Agilent E4980A impedance analyser (Agilent Technologies Inc., CA) over the  $10^3$  to  $10^6$  Hz frequency range with an applied voltage of 100 mV. Electrodes were formed from gold paste fired at 800°C for 2 h on opposing surfaces of the samples. Measurements were made at 30°C intervals from 500°C to ( $T_g - 25^\circ\text{C}$ ). All the measurements were made in air. All impedance data were normalized by the thickness/surface area of each sample. The room temperature impedance was too high to be measured by the impedance analyser. It should be noted that results were not obtained for glass  $Z_{10}B_{13}S_{48}$ . The measured complex impedances ( $Z^*$ ) were used to obtain the conductivity using

$$\sigma = \text{Re}\left(\frac{1}{Z^*}\right) \quad (8)$$

and the dielectric constant using

$$\varepsilon = \text{Re}\left(\frac{1}{i\omega\varepsilon_0 Z^*}\right) \quad (9)$$

where  $\varepsilon_0$  is the permittivity of free space and  $\omega$  is the angular frequency [26].

### 3. Results and discussion

All of the glasses were transparent, free of bubbles and X-ray amorphous. As shown by Table 1 there are some deviations from the batched composition with the  $\text{B}_2\text{O}_3$  content generally being lower than batched reflecting the volatility of this component. As a result other components, especially silica tend to be increased, as compositions have been normalized when determining  $\text{B}_2\text{O}_3$  by difference. It can be seen from Table 1 that  $\text{B}_2\text{O}_3$  losses increase roughly linearly with increasing  $\text{B}_2\text{O}_3$  content reflecting boron volatility at the relatively high melting temperature used. Powder X-ray diffraction (not shown) indicated that all of the samples were X-ray amorphous. Table 2 details the measured values of density,  $T_g$  and TEC for all of the glasses studied. In addition TEC values of the ceramised samples are also given in Table 2.

Table 2: Densities, glass transition temperatures and thermal expansion coefficients (TEC) of all the glasses studied.

Glass code	Measured ZnO/(B <sub>2</sub> O <sub>3</sub> + SiO <sub>2</sub> )	Density /Mg m <sup>-3</sup>	T <sub>g</sub> /°C	TEC /10 <sup>-6</sup> °C <sup>-1</sup>	
				Glass	Glass ceramic
<b>ZnO-B<sub>2</sub>O<sub>3</sub></b>					
Z <sub>18</sub> B <sub>9</sub> S <sub>45</sub>	0.330	4.394	676	8.8	7.5
Z <sub>15</sub> B <sub>10</sub> S <sub>46</sub>	0.274	4.287	674	8.3	8.5
Z <sub>10</sub> B <sub>13</sub> S <sub>48</sub>	0.162	4.207	673	8.2	7.5
Z <sub>9</sub> B <sub>14</sub> S <sub>48</sub>	0.137	4.109	672	7.9	7.2
Z <sub>6</sub> B <sub>16</sub> S <sub>47</sub>	0.101	3.984	670	8.3	7.2
<b>ZnO-SiO<sub>2</sub></b>					
Z <sub>23</sub> B <sub>9</sub> S <sub>40</sub>	0.478	4.504	666	9.2	8.4
Z <sub>21</sub> B <sub>8</sub> S <sub>43</sub>	0.403	4.426	674	9.1	8.2
Z <sub>18</sub> B <sub>9</sub> S <sub>45</sub>	0.341	4.394	676	8.8	7.5
Z <sub>14</sub> B <sub>9</sub> S <sub>48</sub>	0.246	4.357	684	9.0	8.2
<b>Error</b>		± 0.001	± 5	± 0.5	± 0.5

Reflecting the presence of both BaO and La<sub>2</sub>O<sub>3</sub> in these glasses studied the densities are relatively high being of the order of 4-4.5 Mg m<sup>-3</sup> (Table 2). The glass density also increased with increasing ZnO content in both glass series while molar volume decreased (see Figure 1), corresponding to a reduction in oxygen packing density. For the ZnO-B<sub>2</sub>O<sub>3</sub> glass series  $T_g$  was effectively constant within the measurement error. Meanwhile for the ZnO-SiO<sub>2</sub> glass series  $T_g$  increased by ~20°C as the ZnO content decreased from ~23 mol% to ~14 mol% (see Table 2).

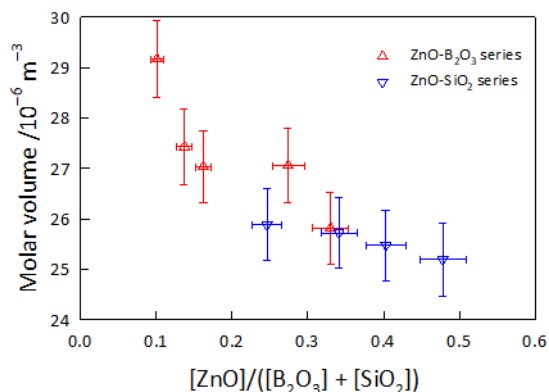


Figure 1: Molar volume versus the measured ratio of ZnO to network forming oxides

Table 2 indicates that in general the thermal expansion coefficients of both the glasses and the corresponding glass-ceramics increase with increasing ZnO content. Also in general the glass-ceramics have lower thermal expansion coefficients than those of the corresponding glasses. However in all cases the values are smaller than  $10.0\text{-}12.0 \times 10^{-6} \text{ K}^{-1}$  range considered ideal for SOFC sealing glasses [27].

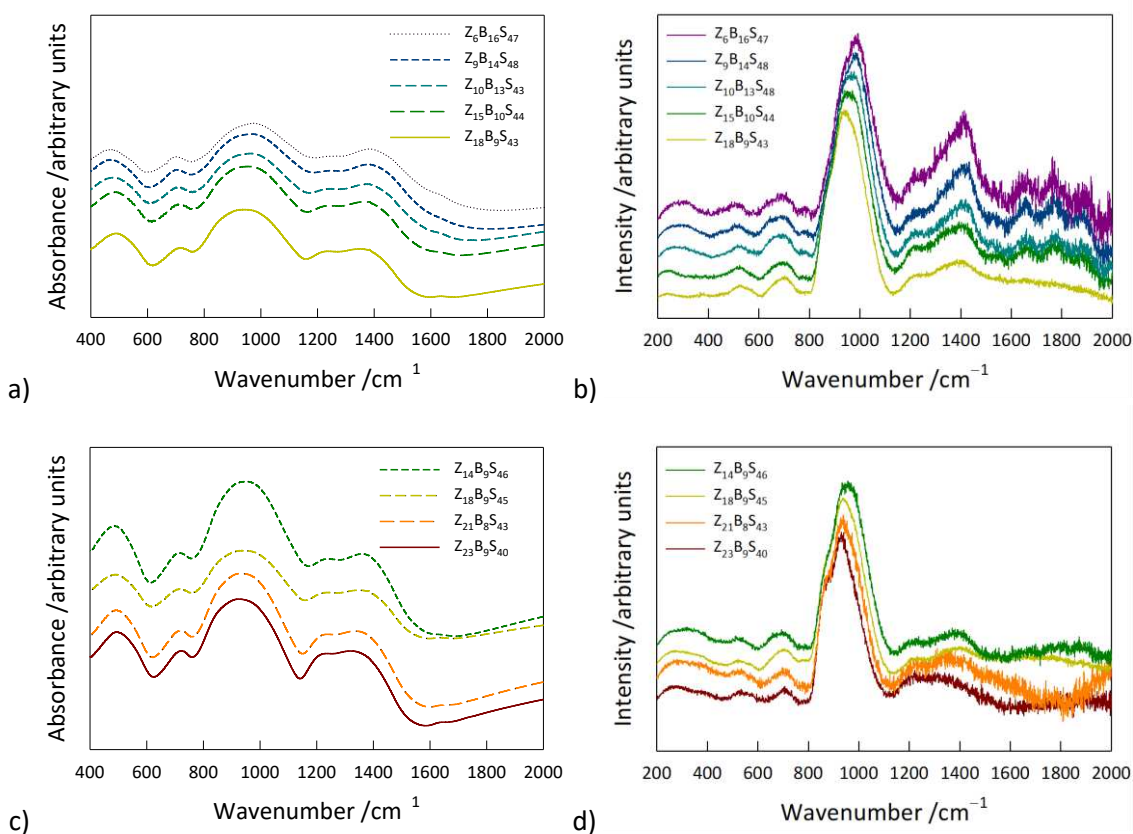


Figure 2: FTIR and Raman spectra of a) and b) ZnO-B<sub>2</sub>O<sub>3</sub> glasses; c) and d) ZnO-SiO<sub>2</sub> glasses. Data offset vertically for clarity

The FTIR and Raman spectra of both series of glasses are shown in Figure 2. Similar features are seen in both sets of spectra with changes in the Raman spectra with composition being more obvious. In particular it can be seen in Figure 2b and d that the Raman peak between  $\sim 800$  and  $\sim 1100 \text{ cm}^{-1}$ ,

which is associated with stretching vibrations of tetrahedral species such as  $\text{SiO}_4$  and  $\text{AlO}_4$ , present in the glass structure, moves to lower wavenumbers as the ZnO content of the glass increases, regardless of whether the silica or the boron oxide content is increasing (see also Figure 3). This suggests that the cross-linking of the tetrahedral species decreases with increasing ZnO content which indicates that ZnO is adopting a network modifier role in the glass structure.

Meanwhile the Raman peak between  $\sim 450$  and  $\sim 550 \text{ cm}^{-1}$  associated with Si-O-Si bending vibrations moves to higher wavenumbers with increasing ZnO content (see Figure 3). Similar shifts are seen in the related FTIR peaks.

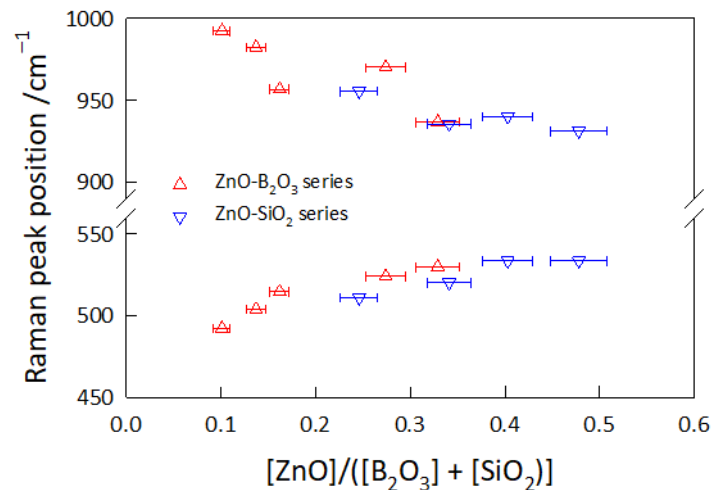


Figure 3: Variation in the peak position of the Raman bands at  $450\text{-}550 \text{ cm}^{-1}$  and  $850\text{-}1000 \text{ cm}^{-1}$  as function of zinc content

In addition Figure 2b shows that the Raman peak at  $\sim 1400 \text{ cm}^{-1}$ , which is associated with the stretching vibration of a  $\text{BO}_3$  bonded to a  $\text{BO}_4$  unit [28], becomes notably more pronounced with increasing  $\text{B}_2\text{O}_3$  content; this is not seen in the ZnO-SiO<sub>2</sub> series of glasses. The Raman band at  $230\text{-}260 \text{ cm}^{-1}$  is assigned to Zn-O bending vibrations in  $\text{ZnO}_4$  tetrahedra; this band shifts to higher wavenumbers with increasing boron oxide content [29].

The changes in Raman peak positions are consistent with the observed behaviour of  $T_g$  for the two glass series. Thus in ZnO-SiO<sub>2</sub> glass series the shift of the Raman peak at  $\sim 1000 \text{ cm}^{-1}$  to higher wavenumbers with decreasing ZnO content (see Figures 2d and 3) coupled with no major changes in the peak at  $\sim 1410 \text{ cm}^{-1}$ , indicates an increase in silica polymerization as ZnO is replaced by SiO<sub>2</sub>, but no significant change in boron oxide polymerization. As a result, as shown in Table 1  $T_g$  decreases with increasing ZnO content for the ZnO-SiO<sub>2</sub> series. In contrast when ZnO is replaced by B<sub>2</sub>O<sub>3</sub> Raman indicates both an increase in polymerization of the silica component shown by the Raman peak at  $\sim 1000 \text{ cm}^{-1}$  again shifting to higher wavenumbers, and a decrease in boron oxide polymerization as shown by the increase in intensity of the Raman peak at  $\sim 1410 \text{ cm}^{-1}$  (see Figure 2b). Thus in this case the lower connectivity of trigonal boron compared to tetragonal boron counters the effects of an increase in silica polymerization, hence there is essentially no change in the observed  $T_g$  values (see Table 2).

Table 3: Measured values of moduli, hardness, indentation fracture toughness and brittleness for all glasses studied

Glass code	$E$ /GPa	$G$ /GPa	$\nu$	$B$ /GPa	$H$ /GPa	$K_{lc}^{indent}$ /MPa m <sup>1/2</sup>	$B_r$ / $\mu\text{m}^{-1/2}$
<b>ZnO-B<sub>2</sub>O<sub>3</sub></b>							
Z <sub>18</sub> B <sub>9</sub> S <sub>45</sub>	92	35.0	0.309	79.7	5.7	0.82	6.9
Z <sub>15</sub> B <sub>10</sub> S <sub>46</sub>	91	34.8	0.305	77.5	5.8	0.87	6.7
Z <sub>10</sub> B <sub>13</sub> S <sub>48</sub>	91	34.9	0.307	78.8	5.8	0.85	6.9
Z <sub>9</sub> B <sub>14</sub> S <sub>48</sub>	88	33.6	0.304	74.5	5.9	0.88	6.7
Z <sub>6</sub> B <sub>16</sub> S <sub>47</sub>	88	33.6	0.303	74.3	5.8	0.88	6.6
<b>ZnO-SiO<sub>2</sub></b>							
Z <sub>23</sub> B <sub>9</sub> S <sub>40</sub>	91	34.8	0.311	80.7	5.8	0.80	7.3
Z <sub>21</sub> B <sub>8</sub> S <sub>43</sub>	91	34.4	0.316	82.2	5.7	0.77	7.4
Z <sub>18</sub> B <sub>9</sub> S <sub>45</sub>	92	35.0	0.309	79.7	5.7	0.82	6.9
Z <sub>14</sub> B <sub>9</sub> S <sub>48</sub>	91	34.6	0.311	80.0	5.8	0.80	7.3
<b>Error</b>	$\pm 2$	$\pm 0.1$	$\pm 0.007$	$\pm 0.5$	$\pm 0.3$	$\pm 0.01$	$\pm 0.3$

While there are no particular targeted values for the mechanical properties of sealing glasses however they must be mechanically capable of ensuring gas tightness and adhesion during sealing and operation at dual atmosphere and high temperatures.

Table 3 summarises the measured mechanical properties for all of the glasses studied. The Young's moduli and Poisson's ratios are relatively high compared to many silicate glasses, with the Poisson's ratio values suggesting high atomic packing density ( $C_g$ ) values of  $\sim 0.6$  [30] whereas the calculated  $C_g$  values for these glasses are  $\sim 0.5$ . This may suggest that the "S" shaped dependence of Poisson's ratio on  $C_g$  observed by Rouxel [30] does not always apply; it is worth noting that a similarly high Poisson's ratio has recently been reported for a cesium aluminoborate glass [31]. Similarly high (or higher) Young's moduli have been reported for some magnesia containing lanthanum aluminoborates and aluminoborosilicates investigated as potential sealing glasses [32]. The changes in moduli with composition seen here are small with no obvious dependence on silica content in the ZnO-SiO<sub>2</sub> glass series, although there is a reduction in all three of Young's, shear and bulk moduli with increasing boron content in the ZnO-B<sub>2</sub>O<sub>3</sub> glass series. The hardness values (see

Table 3) are in line with values reported for some sealant glasses [33] but lower than those reported by Rodríguez-López *et al.* [8] for BaO/SrO-MgO-B<sub>2</sub>O<sub>3</sub>-SiO<sub>2</sub> sealant glasses; this probably reflects the presence of La<sub>2</sub>O<sub>3</sub> in these glasses. Essentially no change in hardness with composition was seen for either glass series.

In principle relatively high Young's moduli could be expected to result in relatively high fracture toughness values, assuming no major variation in the surface energy term. Some of the indentation fracture toughness values reported here are indeed relatively high for glasses (see

Table 3 and Figure 4); however it is known that indentation fracture toughness measurements do not always correlate directly with more conventional fracture toughness measurement [34] and as shown in Figure 4a the glass with highest indentation toughness actually has the lowest measured Young's modulus. Figure 4b shows that the indentation fracture toughness values tend to decrease with increasing Poisson's ratio in these glasses; similar behaviour has been reported by Barlet *et al.*

[35].  $E/H$  values are  $\sim 15$ - $16$ , similar values have been reported for other borosilicates albeit with lower Poisson's ratio values [36].

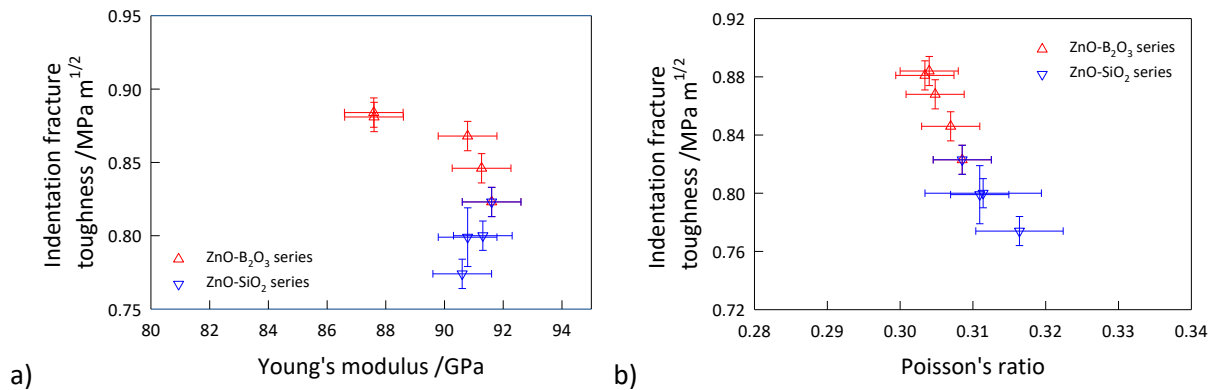


Figure 4: Indentation fracture toughness versus a) Young's modulus and b) Poisson's ratio for both series of glasses

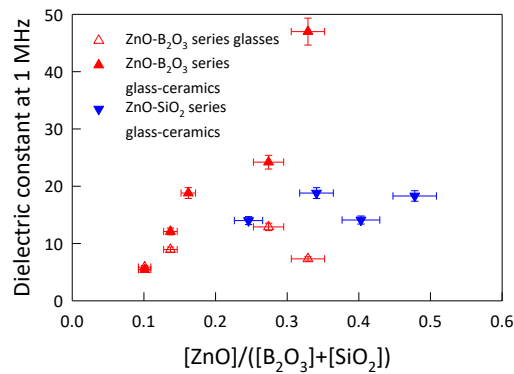


Figure 5: Dielectric constant at 600-610°C measured at 1 MHz versus the measured ratio of ZnO to network forming oxides for the ZnO-B<sub>2</sub>O<sub>3</sub> series glasses and glass-ceramics and for the ZnO-SiO<sub>2</sub> series glass-ceramics

Since the applications of these sealing glasses will be at temperatures above their  $T_g$  the conductivity and dielectric constants as a function of composition were measured at temperatures around 600°C. Figure 5 shows the dielectric constant at 1 MHz versus composition for the ZnO-B<sub>2</sub>O<sub>3</sub> and all of the ceramised samples. It can be seen that in general the dielectric constant increases with increasing ZnO content reflecting the higher polarizability of  $\text{Zn}^{2+}$  compared to the network formers that it is replacing in these compositions [37,38]. It is unclear why the  $\text{Z}_{18}\text{B}_9\text{S}_{45}$  glass ceramic sample apparently has a significantly higher dielectric constant than the other samples. For the ZnO-B<sub>2</sub>O<sub>3</sub> series it was found that the glass ceramics are more conductive than their parent glasses (see also Figure 6). Impedance data suggests that the grains are more conductive than the grain boundaries.

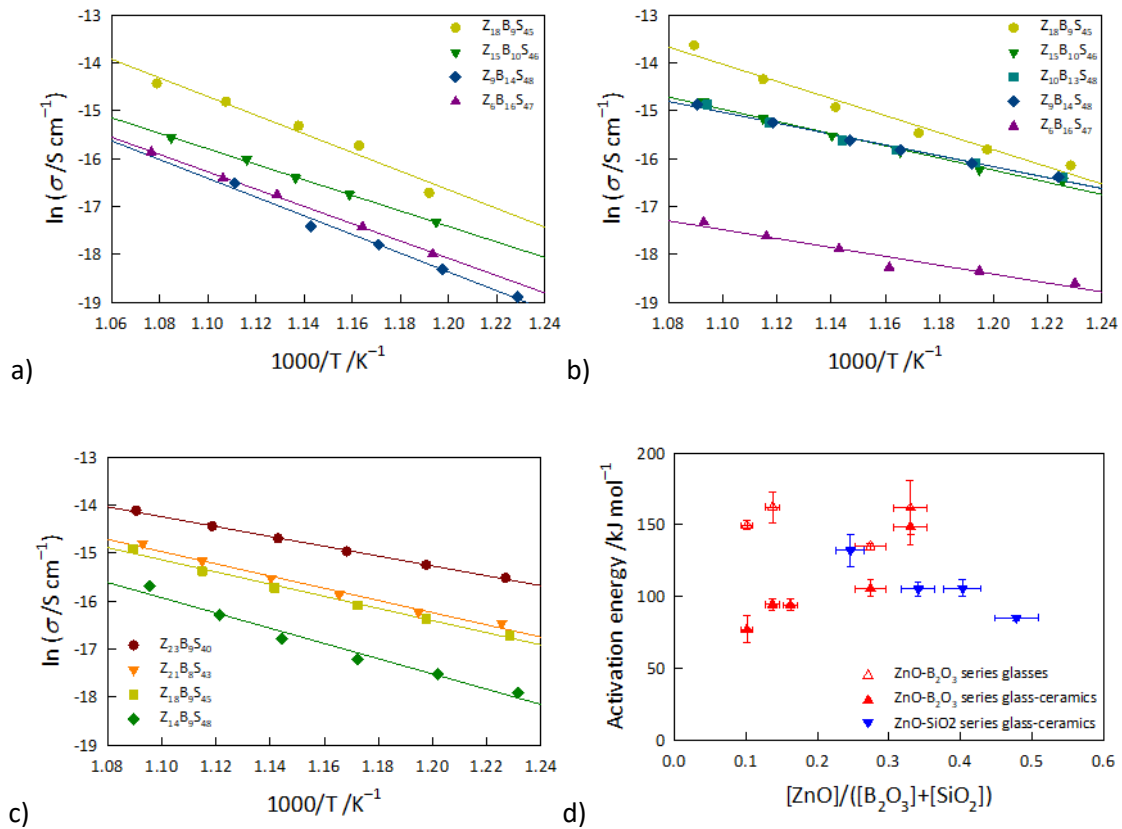


Figure 6: Arrhenius activation energy plots for a) ZnO-B<sub>2</sub>O<sub>3</sub> series glasses; b) ZnO-B<sub>2</sub>O<sub>3</sub> series glass ceramics; c) ZnO-SiO<sub>2</sub> series glass ceramics and d) calculated activation energy versus the measured ratio of ZnO to network forming oxides for the ZnO-B<sub>2</sub>O<sub>3</sub> series glasses and glass-ceramics and for the ZnO-SiO<sub>2</sub> series glass-ceramics

Figure 6a and b shows that the electrical conductivity of both ZnO-B<sub>2</sub>O<sub>3</sub> series glasses and glass-ceramics increases with increasing temperature and increasing ZnO content. The measured ac conductivities were found to be essentially constant over the frequency range 10<sup>3</sup> and 10<sup>4</sup> Hz and the reported values are averages obtained over that range. Similarly Figure 6c shows that the conductivity of ZnO-SiO<sub>2</sub> glass-ceramics also increases with increasing temperature and ZnO content. The FTIR and Raman results indicate that ZnO is acting in a network modifier role in these glasses and thus an increase in ZnO increases the presence of more mobile network modifier ions (Zn<sup>2+</sup> and Ba<sup>2+</sup>) in the glass hence the conductivity is increased [39]. The activation energy for electrical conduction is lower for the glass-ceramics than for the corresponding parent glasses (see Figure 6d), presumably due to increased conductivity of the lanthanum borosilicate crystal phase; the impedance measurements indicate that the crystals are more conductive than the residual glass. In the glassy state the activation energy for conduction does not change significantly with composition. For the ZnO-SiO<sub>2</sub> series glass ceramic the activation energy for conduction tends to decrease with increasing ZnO content (see Figure 6d).

## Conclusions

Two series of BaO-ZnO-La<sub>2</sub>O-Al<sub>2</sub>O<sub>3</sub>-B<sub>2</sub>O<sub>3</sub>-SiO<sub>2</sub> glasses have been studied in which ZnO replaced either B<sub>2</sub>O<sub>3</sub> or SiO<sub>2</sub>. *T<sub>g</sub>* decreased with increasing ZnO content in the ZnO-SiO<sub>2</sub> glasses but there was little variation in *T<sub>g</sub>* in the ZnO-B<sub>2</sub>O<sub>3</sub> glasses. Both series of glasses had relatively high densities due to the presence of both BaO and La<sub>2</sub>O<sub>3</sub> oxides and molar volume decreased with increasing ZnO content; this along with the Raman and FTIR evidence points to ZnO acting in a network modifier role. The

Young's moduli values are relatively high compared to many silicate glasses however they are in line with ones reported for some lanthanum aluminoborate and aluminoborosilicate glasses developed for similar applications [32]. Indentation toughness gave some high values for glasses which suggests that these glasses will be relatively resistant to fracture. The thermal properties of these glasses are lower than the required value for SOFCs applications however their electrical insulation capabilities are comparable to the values required for sealing glasses. The compositions with lowest electrical conductivities are those with lowest zinc oxide content. Of the glasses studied 9.74BaO-6.39ZnO-15.84La<sub>2</sub>O<sub>3</sub>-5.04Al<sub>2</sub>O<sub>3</sub>-15.63B<sub>2</sub>O<sub>3</sub>-47.37SiO<sub>2</sub> (Z<sub>6</sub>B<sub>16</sub>S<sub>47</sub>) has the most promising properties for SOFC sealing applications.

## Acknowledgments

This work was conducted whilst LUG was in receipt of a studentship from TETFund, Nigeria. We thank Drs Lisa Hollands, Fan Yang and Nik Reeves-McLaren for their help with glass melting, impedance spectroscopy and XRD/Raman measurements respectively.

## References

- [1] Zhao, Y. and Malzbender J., *Elevated temperature effects on the mechanical properties of solid oxide fuel cell sealing materials*. J. Power Sources, 2013. **239** 500-504.
- [2] Malzbender, J., Zhao Y. and Beck T., *Fracture and creep of glass-ceramic solid oxide fuel cell sealant materials*. J. Power Sources, 2014. **246** 574-580.
- [3] Laorodphan, N., Namwong P., Thiemsorn W., Jaimasith M., Wannagon A. and Chairuang Sri T., *A low silica, barium borate glass-ceramic for use as seals in planar SOFCs* J. Non-Cryst. Solids 2009 **355** 38-44
- [4] Chang, H-T., Lin C-K. and Liu C-K., *Effects of crystallization on the high-temperature mechanical properties of a glass sealant for solid oxide fuel cell*. J. Power Sources, 2010. **195** 3159-3165.
- [5] Chang, H-T., Lin C-K., Liu C-K. and Wu S-H., *High-temperature mechanical properties of a solid oxide fuel cell glass sealant in sintered forms*. J. Power Sources, 2011. **196** 3583-3591.
- [6] Wang, R., Lü Z., Liu C., Zhu R., Huang X., Wei B., Ai A. and Su W. *Characteristics of a SiO<sub>2</sub>-B<sub>2</sub>O<sub>3</sub>-Al<sub>2</sub>O<sub>3</sub>-BaCO<sub>3</sub>-PbO<sub>2</sub>-ZnO glass-ceramic sealant for SOFCs*. J. Alloys Compounds, 2007. **432** 189-193.
- [7] Coillot, D., Méar, F.O., Nonnet, H. and Montagne, L., *New viscous sealing glasses for electrochemical cells*. Int. J. Hydro. Energy, 2012 **37** 9351-9358
- [8] Rodríguez-López S., Wei J., Laurenti K.C., Mathias I., Justo V.M. Serbena F.C., Baudin C., Malzbender J. and Pascual M.J. *Mechanical properties of solid oxide fuel cell glass-ceramic sealants in the system BaO/SrO-MgO-B<sub>2</sub>O<sub>3</sub>-SiO<sub>2</sub>* J. Europ. Ceram. Soc. 2017 **37** 3579-3594
- [9] Reis, S.T. and Brow R.K., *Designing sealing glasses for solid oxide fuel cells*. J. Mater. Engng. Perf., 2006. **15**(4): p. 410-413.
- [10] Wang, S-F., Wang Y-R., Hsu Y-F. and Chuang C-C. *Effect of additives on the thermal properties and sealing characteristic of BaO-Al<sub>2</sub>O<sub>3</sub>-B<sub>2</sub>O<sub>3</sub>-SiO<sub>2</sub> glass-ceramic for solid oxide fuel cell application*. Int. J. Hydro. Energy, 2009 **34** 8235-8244.
- [11] Sasmal, N., Garai M., Rahman Molla A., Tarafder A., Prakash Singh S. and Karmakar B., *Effects of lanthanum oxide on the properties of barium-free alkaline-earth borosilicate sealant glass* J. Non-Cryst. Solids 2014 **387** 62-70.
- [12] Sun, T., Xiao, H., Guo, W. and Hong, X., *Effect of Al<sub>2</sub>O<sub>3</sub> content on BaO-Al<sub>2</sub>O<sub>3</sub>-B<sub>2</sub>O<sub>3</sub>-SiO<sub>2</sub> glass sealant for solid oxide fuel cell*. Ceramics International, 2010. **36**(2): p. 821-826.
- [13] Hsiu-Tao Chang, C.-K. Lin, Chien-Kuo Liu, *High Temperature Mechanical Properties of a Crystallized BaO-B<sub>2</sub>O<sub>3</sub>-Al<sub>2</sub>O<sub>3</sub>-SiO<sub>2</sub> Glass Ceramic for SOFC*, in ASME 2009: Newport Beach, California, USA.

- [14] Zhao, Y., Malzbender J., and Gross S.M. *The effect of room temperature and high temperature exposure on the elastic modulus, hardness and fracture toughness of glass ceramic sealants for solid oxide fuel cells*. J. Europ. Ceram. Soc., 2011. **31**(4): p. 541-548.
- [15] Mahapatra M.K. and Lu K. *Glass-based seals for solid oxide fuel and electrolyzer cells - A review*. Materials Science & Engineering Reports, 2010 **67** 65-85.
- [16] Tulyaganov D.U., Amarnath Reddy A., Kharton V.V. and Ferreira J.M.F, *Aluminosilicate-based sealants for SOFCs and other electrochemical applications - A brief review*. J. Power Sources 2013 **242** 486-502.
- [17] Fergus, J.W., *Sealants for solid oxide fuel cells*. Journal of Power Sources, 2005. **147**: p. 46-57.
- [18] Larsen, P.H., F.W. Poulsen, and R.W. Berg, *The influence of SiO<sub>2</sub> addition to 2MgO–Al<sub>2</sub>O<sub>3</sub>–3.3P<sub>2</sub>O<sub>5</sub> glass*. J. Non-Cryst. Solids, 1999 **244** 16-24.
- [19] Goel, A., Tulyaganov D.U., Goel I.K., Shaaban E.R. and Ferreira J.M.F *Effect of BaO on the crystallization kinetics of glasses along the Diopside–Ca-Tschermak join*. J. Non-Cryst. Solids, 2009 **355** 193-202.
- [20] Lahl, N., Singh, K., Singheiser, L., Hilpert, K. and Bahadur, D., *Crystallisation kinetics in AO–Al<sub>2</sub>O<sub>3</sub>–SiO<sub>2</sub>–B<sub>2</sub>O<sub>3</sub> glasses (A = Ba, Ca, Mg)*. J. Mater. Sci., 2000. **35** 3089-3096.
- [21] Ojha, P.K., Chongdar, T.K., Gokhale, N.M. and Kulkarni, A.R., *Physical and thermal behaviour of Sr-La-Al-B-Si based SOFC glass sealants as function of SrO content and B<sub>2</sub>O<sub>3</sub> ratio in the matrix*. J. Power Sources, 2011. **196** 4594-4598
- [22] Timurkutluk, B., Timurtutluk, C., Mat, M.D. and Kaplan Y., *A review on cell/stack designs for high performance solid oxide fuel cells*. Renew. Sustain. En. Rev., 2016. **56** 1101-1121
- [23] Colomban, P., Tournie A. and Bellot-Gurlet L., *Raman identification of glassy silicates used in ceramics, glass and jewellery: a tentative differentiation guide*. J. Raman Spect., 2006. **37** 841-852.
- [24] Mysen, B.O., Finger, L.G., Virgo, D. and Seifert, F.A. *Curve-fitting of Raman spectra of silicate glasses*. Amer. Min., 1982. **67** 686-695
- [25] Ponton, C.B., and Rawlings, R.D., *Vickers indentation fracture toughness test Part 2: Application and critical evaluation of standardized indentation toughness equations* Mater. Sci. Technol. 1989. **5** 961-976
- [26] Zang, J., Li, M., Sinclair, D.C., Jo, W. and Rödel, J., *Impedance spectroscopy of (Ba<sub>1/2</sub>Na<sub>1/2</sub>)TiO<sub>3</sub>–BaTiO<sub>3</sub> ceramics modified with (K<sub>0.5</sub>Na<sub>0.5</sub>)NbO<sub>3</sub>*. J. Amer. Ceram. Soc., 2014. **97** 1523-1529
- [27] Hao, J., Zan, Q., Ai, D., Ma, J., Deng, C. and Xu, J., *Structure and high temperature physical properties of glass seal materials in solid oxide electrolysis cell*. J. Power Sources, 2012. **214** 75-83
- [28] Manara, D., Grandjean, A., and Neuville, D.R., *Advances in understanding the structure of borosilicate glasses: A Raman spectroscopy study* Amer. Min., 2009. **94** 777-784
- [29] Yadav, A.K., and Singh, P., *A review of the structures of oxide glasses by Raman spectroscopy*. RSC Adv. 2015. **5** 67583
- [30] Rouxel T. *Elastic Properties and Short-to Medium-Range Order in Glasses*. J. Amer. Ceram. Soc. 2007. **90** 3019-3039
- [31] To T., Jensen L.R., and Smedsjaer M.M., *On the relation between fracture toughness and crack resistance in oxide glasses* J. Non-Cryst. Solids, 2020 **534** 119946
- [32] Ghosh S., Sharma, A.D., Mukhopadhyay, A.K., Kundu, P., and Basu, R.N., *Effect of BaO addition on magnesium lanthanum alumino borosilicate-based glass-ceramic sealant for anode-supported solid oxide fuel cell* Int. J. Hydrogen Energy, 2010 **35** 272-283
- [33] Kothiyal G.P., Goswami M., Tiwari B., Sharma K., Ananthanarayanan A. and Montagne L. *Some recent studies on glass/glass-ceramics for us as sealants with special emphasis for high temperature applications* J. Adv. Ceram. 2012 **1** 110-129
- [34] Kiliñç E. and Hand R.J. *Mechanical properties of soda–lime–silica glasses with varying alkaline earth contents* J. Non-Cryst. Solids, 2015 **429** 190–197

- [35] Barlet M., Delaye J-M. Charpentier T., Gennisen M., BonamyD., Rouxel T. and Rountree C.L. *Hardness and toughness of sodium borosilicate glasses via Vickers's indentations*. J. Non-Cryst. Solids, 2015 **417** 66-79
- [36] Rouxel T. *Driving force for indentation cracking in glass: composition, pressure and temperature dependence* Phil. Trans. R. Soc. A 2015 **373** 20140140
- [37] Duffy J.A., *The electronic polarisability of oxygen in glass and the effect of composition* J. Non-Cryst. Solids, 2002 **297** 275-284
- [38] Wang Z., Hu Y, Lu H. and Yu F. *Dielectric properties and crystalline characteristics of borosilicate glasses* J. Non-Cryst. Solids 2008 **354** 1128-1132
- [39] Lara C., Pascual M.J., Keding R. and Durán A. *Electrical behaviour of glass-ceramics in the systems RO-BaO-SiO<sub>2</sub> (R = Mg, Zn) for sealing SOFCs* J. Power Sources 2006 **157** 377-384